







Article

Thermal Lattice Field during Ultra-Short Laser Pulse Irradiation of Metal Targets: A Fokker–Planck Analytical Model

Sinziana-Andreea Anghel ^{1,2}, Mihai Oane ^{1,*} , Cristian N. Mihăilescu ¹, Bogdan A. Sava ^{1,3} , Mihail Elişa ⁴, Natalia Mihăilescu ^{1,*}, Dorina Ticoş ¹, Alexandra M. I. Trefilov ^{1,*} , Carmen Ristoscu ¹ , Ana V. Filip ¹  and Ion N. Mihăilescu ^{1,*} 

¹ National Institute for Laser, Plasma and Radiation Physics (INFLPR), Ilfov, 077125 Magurele, Romania; sanziana.anghel@inflpr.ro (S.-A.A.); cristi.mihailescu@inflpr.ro (C.N.M.); bogdan.sava@inflpr.ro (B.A.S.); dorina.toader@inflpr.ro (D.T.); carmen.ristoscu@inflpr.ro (C.R.); ana.filip@inflpr.ro (A.V.F.)

² Faculty of Physics, University of Bucharest, Ilfov, 077125 Magurele, Romania

³ Faculty of Applied Chemistry and Materials Science, University Politehnica Bucharest, 313 Spl. Independentei, 060042 Bucharest, Romania

⁴ National Institute R&D for Optoelectronics, INOE 2000, 409 Atomistilor Str, Ilfov, 077125 Magurele, Romania; elisa@inoe.ro

* Correspondence: mihai.oane@inflpr.ro (M.O.); natalia.serban@inflpr.ro (N.M.); alexandra.trefilov@inflpr.ro (A.M.I.T.); ion.mihailescu@inflpr.ro (I.N.M.)

Abstract: The ultrafast fs laser pulse heating of thin metal films is studied for the first time using the two-temperature model on the basis of the Fokker–Planck formalism. The incident laser radiation is multi-modal, while the electron temperature is described during the first 2 fs. The predictions are intended for use by experimentalists in optoelectronics, photonics, laser processing, electronics, and bio- and nanomedicine. The crucial role of the nano-sized spatial dimensions of the metal sample is highlighted. A significant result of this study is the interdependence between the target's size, the phonon/lattice characteristics, and the coefficient β (the quotient of non-diffusive phenomena), which varies between zero (pure diffusive case) and one (pure non-diffusive case).

Keywords: two-temperature model; Fokker–Planck analytical approach; laser heating of metals; fs laser pulses; analytical simulations; β parameter



Citation: Anghel, S.-A.; Oane, M.; Mihăilescu, C.N.; Sava, B.A.; Elişa, M.; Mihăilescu, N.; Ticoş, D.; Trefilov, A.M.I.; Ristoscu, C.; Filip, A.V.; et al. Thermal Lattice Field during Ultra-Short Laser Pulse Irradiation of Metal Targets: A Fokker–Planck Analytical Model. *Metals* **2023**, *13*, 1775. <https://doi.org/10.3390/met13101775>

Academic Editor: Milan Brandt

Received: 19 September 2023

Revised: 17 October 2023

Accepted: 18 October 2023

Published: 20 October 2023



Copyright: © 2023 by the authors. Licensee MDPI, Basel, Switzerland. This article is an open access article distributed under the terms and conditions of the Creative Commons Attribution (CC BY) license (<https://creativecommons.org/licenses/by/4.0/>).

1. Introduction

The laser heating of metals is a dynamic research field that was initiated along with the debut of lasers in the early 1960s. It has had a continuous evolution since then, in particular from the first continuous wave to pulsed laser systems, generating trains of pulses of shorter and shorter duration (τ). This “explosion” has already extended to fs, and now laser pulses simultaneously cover both the experimental and theoretical domains [1–3]. It was thus shown that the process evolution in a chemically ambient fluid (e.g., air or atmospheres of any sort) provides positive feedback, generally leading to the acceleration of the oxidation processes and an overall increase in the induced temperatures [4]. It is, however, generally accepted that the laser radiation/field is coupling, in this case, to electrons [4]. Studies are presently mainly intended to pave the way towards higher-performance technologies with minimal losses and low prices in top R&D fields like bio-nanomedicine, optoelectronics, communications, and bio-chemistry, among many others [4–6].

Phenomena in solid-state physics, including electronic and thermal transport, superconductivity, spin caloritronics, and laser-induced phase transitions, require a more profound understanding of the fundamental scattering processes, as expressed by interactions between lattice vibrations and electrons. In the case of ultra-short laser pulses, the substantial difference in heat capacity between electrons/phonons and the lattice is the source of the selective perturbation which allows the direct observation of electron gas

scattering processes. The interaction therefore requires appropriate developments in this case to describe the features of this very complex process. This is the main objective of this contribution, and for the sake of a better understanding of the mathematical model and numerical simulations on this basis, the main physical quantities involved in this study are collected in Table 1.

Table 1. Physical quantities in the present study.

Symbol	Name of Physical Quantity	International Unit of Measurement
X	Cartesian space coordinate	m
Y	Cartesian space coordinate	m
Z	Cartesian space coordinate	m
t	Time	s
C_e	Caloric capacities for electrons	J/(kg·K)
K_e	Thermal conductivity for electrons	W/(m·K)
C_l	Caloric capacities for lattice	J/(kg·K)
K_l	Thermal conductivity for lattice	W/(m·K)
G	Electron–phonon coupling factor	W/(m ³ ·K)
S	Source term	J/(m ³ ·s)
T_e	Electron temperature	K
T_l	Lattice temperature	K
R	Target reflectivity	%
F	Laser fluence	J/m ²
$H_{m,n}$	Hermite polynomials of order m and n	Real number
$w_{x,y}$	1/e radii of the laser spot (beam waist) along x and y directions	m
z_s	Maximum penetration length after one laser pulse	m
δ	Optical penetration depth	m
δ_b	Non-diffusive length	m
t_l	Irradiation time	s
γ	Thermal diffusivity	m ² /s
τ	Laser–Au relaxation time	s
α	1/ τ	s ^{−1}
ξ	Increment (real number)	Real number
φ	Phase function	Real number
β	Coefficient indicating the proportion of non-diffusive phenomenon	Real number between 0 and 1
$f(x)$	From $T_l(x, 0)$	K
σ	Increment (real number)	Real number
L	Total thickness	nm
R	$R = z/L$, where z is the depth inside the thin film and L the total thickness	a.u.
ρ	Mass density	Kg/m ³

The energy relaxation and conversion processes between electrons and vibration systems can be monitored in real time using thermo-modulation spectroscopy techniques. Therefore, it was not difficult to monitor the non-equilibrium between electrons and vibration states in metals using short-pulsed time-domain thermo-reflectance (TDTR). This confirmed earlier theories based upon the assumption that the electrons/phonons and lattice could be described by two different temperatures and validated the two-temperature model (TTM) developed by Anisimov [7]. Namely, the TTM consists of two coupled heat equations: one for electrons/phonons and one for the lattice. At the fs scale, one good approximation can imply a separation of the two equations of the TTM, i.e., of T_e (electron temperature) and T_l (lattice phonon temperature) [8]. It should be noted that in the case of dielectrics and semiconductors, multiphoton absorption plays a significant role.

In particular, femtosecond laser pulses are appropriate to resolve the time required for the electronic system to transfer its energy to the lattice, allowing for the inferring of the electron–phonon coupling (G), i.e., the volumetric energy rate. It has been shown [9] that the laser–matter interaction can be classified as non-thermal for $\tau \geq 10^{-15}$ s and $\tau \leq 10^{-13}$ s and as thermal for longer durations. In fact, any non-thermal process starts with the absorption of radiation in the femto- and atto-second range.

Therefore, all the above studies assumed that electron thermalization takes place on a time scale shorter than the laser pulse duration. In contrast to the theoretically calculated Fermi relaxation time of 40 fs, Fann et al. [10] showed that in photoemission measurements the thermalization time of the electron gas in Au is 1 ps, which is comparable to the electron–phonon (e - p) relaxation time. This is supported by pump–probe femtosecond measurements, which have also revealed a long-lived non-Fermi distribution of electrons in Au on the order of the e - p relaxation time. A recent computational study also showed that the thermalization time of the electron gas can range from 10 fs to picoseconds, depending on the laser irradiance [11]. The electron temperature can be considered “effective” since the time required for the electron gas to relax to a Fermi distribution is of the order of the e - p relaxation time.

On the other hand, the effect of electron–electron (e - e) thermalization on the e - p coupling has not yet been rigorously studied for the absorption of high fluences and large e - p non-equilibria. This led the way to more than 20 years of experimental investigation of e - p coupling dynamics during non-equilibrium. As a consequence, the non-thermal electron–phonon interaction behavior during high-energy, short-pulse laser heating experiments have not yet been well quantified. Specifically, the dynamics of the e - e interactions influencing the e - p relaxation were investigated via electron relaxation in thin Au films over a wide range of lattice temperatures (77–300 K) and absorbed laser fluences using TDTR. Au’s weak electron–lattice interaction strength for its relatively long Fermi relaxation time has well-characterized band structures and intensively studied thermal properties and transport dynamics that were brought together in an improved output to survey the e - p relaxation mechanisms at high electron temperatures with large laser perturbations.

A quasi-linear dependence of the electron relaxation rate on the lattice temperature increase has been reported for the low perturbation limit of the electron system [12]. For large fluences and higher degrees of e - p non-equilibrium, the lattice temperature dependence on G is much less pronounced and becomes nearly constant for the largest fluences.

Two-temperature models (TTMs) were recently widely disseminated to describe laser–metal interactions [4,6,13–17]. High-energy electrons are generated. Then, in a “cold” crystalline network, a phenomenon accurately described via TTMs is governed by the “balance” between the flow of excited electrons and the network, as expressed by the electron–phonon coupling.

Non-linear TTM equations can be written in this case as follows:

$$C(T_e) = \nabla[k_e(T_e, T_l)\nabla T_e] - G(T_e)(T_e - T_l) + S(X, Y, Z, t) \quad (1)$$

And

$$C(T_l)T_l = \nabla[k_l(T_l)\nabla T_l] + G(T_e)(T_e - T_l) \quad (2)$$

Here, t is the current time, while X , Y , and Z are the Cartesian space coordinates, and $C_{e,l}$ and $k_{e,l}$ are the caloric capacities and the thermal conductivities for electrons (e) and lattice/phonons (l), respectively. G stands for the electron–phonon coupling factor, while S is the source term in the laser–target interaction [18]. G thus quantifies the volumetric rate of energy transfer between the two states.

A new model is proposed, which allows for a focus on diffusive and non-diffusive phenomena based upon the Fokker–Planck formalism applied to the second equation of the TTM.

In a diffusive case, the heat is transferred from higher- to lower-temperature regions. The non-diffusive phenomena refer to the cases when the photons cross the target without any interaction. The factor β introduced by the Fokker–Planck model describes the balance between diffusive and non-diffusive phenomena.

Transient heat transport is mainly performed by phonons. Although the behaviors of different phonons are often considered independent, phonon transport depends on their mean path. In the case of short Mean Free Paths (MFPs), the phonon transport is non-diffusive and becomes diffusive for long MFPs, while the opposition originates from

scattering processes experienced by phonons. The two transport regimes coexist, however, in many cases of interest. Depending on the temperature gradients, the photons obey the following order: non-diffusive phonons < diffusive phonons. Non-diffusive–diffusive phonon transport is expected to occur in nanoscale structures, making both low-dimensional and nanoscale effects possible. The significance of non-diffusive–diffusive transport phonons results in a large amplitude of tuning of the heat flux [15,18–20].

Based on previous results, we applied two semi-analytical numerical methods of integral transformations on finite domains to solve the TTM [21]. However, a comparison with experimental values was extremely difficult in this case due to the ultra-short duration of the laser pulses (within the $(10^{-15}–10^{-13})$ s range) as well as the uncertainty introduced by the substantial Heat-Affected Zone (HAZ) of $\geq 10^{-7}$ m, i.e., more than 100 nm. That is why theoretical and computational physics should be used in this field as a simple and reliable, if not unique, approach.

We recently managed to solve Equations (1) and (2) using integrated transformations on finite domains in combination with some experimental data [22]. The analysis has been extended to include TTM solutions for the case under examination. Namely, we considered the interaction of multi-mode laser pulses of fs duration with metallic (Au) targets. To solve the heat equation, we used the technique of heat operators [5,23].

2. Mathematical Modeling of Electronic Thermal Fields

If one considers flash laser irradiation by a single very short pulse, $T_e \gg T_l$ and consequently:

$$\frac{\partial^2 T_e}{\partial x^2} + \frac{\partial^2 T_e}{\partial y^2} + \frac{\partial^2 T_e}{\partial z^2} = \frac{1}{\gamma} \frac{\partial T_e}{\partial t} - \frac{S}{k_e} + \left(\frac{G}{k_e} \right) T_e \quad (3)$$

where γ and ρ are the thermal diffusivity and the mass density of the target, respectively, and G stands for the electron–photon coupling factor.

One should mention here the shielding effect of the generated laser plasma, which might cause a slowdown of the ablation rate/heating effect [1]. In this process, one fraction of the incident laser energy is absorbed by free electrons. The relaxation time of this phenomenon is usually in the 100 fs range. Due to the difference in free electrons, the heavy ions in the plasma cannot significantly absorb laser radiation. This is because the field oscillations act quicker than those of the heavy ions. The electron–phonon relaxation time is therefore superior to that of the collision of electrons or ions. That is why the laser irradiation of metals with fs laser pulses is often described as phonon lattice cooling.

Therefore, we further use 1 fs for the laser pulse duration, which allows us to design a generalized model to describe the thermal distribution in the metal after laser irradiation.

Next, we introduce the term S in accordance with the Lambert–Beer law:

$$S(X, Y, Z, t) = \sum_{m,n} \sqrt{\frac{4 \ln 2}{\pi}} \frac{(1-R)F}{t_p(\delta + \delta_b)} \left[H_m \left(\frac{\sqrt{2} x}{w_x} \right) \exp \left(-\frac{x^2}{w_x^2} \right) \right]^2 \cdot \left[H_n \left(\frac{\sqrt{2} y}{w_y} \right) \exp \left(-\frac{y^2}{w_y^2} \right) \right]^2 \exp \left(-\frac{z - z_s}{\delta + \delta_b} \right) \exp \left[-4 \ln 2 \left(\frac{t - 2t_p}{t_p} \right)^2 \right] \quad (4)$$

Here, $H_{m,n}$ are Hermite polynomials of order m and n ; R is the target reflectivity; δ is the optical penetration depth; δ_b is the non-diffusive length; F is the laser fluence; and $w_{x,y}$ are the $1/e$ radii of the laser spot (beam waist) along the x and y directions, respectively, while z_s is the maximum penetration length after one laser pulse.

To pin down ideas, one may consider one variable only; let us say x . In Figures 1–5 it is considered that the target is a Au thin film that has a $Z_{\max} = 20$ nm (the thickness of

the thin film is 20 nm, and z is the direction of the laser propagation). In this case, the generalized heat equation takes the following form:

$$\frac{\partial T_e(x, y, z, t)}{\partial t} = \gamma \frac{\partial^2 T_e(x, y, z, t)}{\partial x^2} + \alpha T_e(x, y, z, t) \quad (5)$$

with the solution

$$T_e(x, y, z, t) = e^{t\alpha} \frac{C}{2\sqrt{\pi\alpha t}} \int_{-\infty}^{+\infty} e^{-\frac{(x-\sigma)^2}{4t\alpha}} \left(\exp \left[-2 \left(\frac{\sigma}{w_x} \right)^2 H_m \left(\frac{\sqrt{2}\sigma}{w_x} \right) \right]^2 \right) d\sigma \quad (6)$$

$$C \equiv \sqrt{\frac{4\ln 2}{\pi}} \frac{1-R}{t_l(\delta + \delta_b)} \left[H_n \left(\frac{\sqrt{2}y}{w_y} \right) \exp \left(-\frac{y^2}{w_y^2} \right) \right]^2 \exp \left(-\frac{z-z_s}{\delta + \delta_b} \right) \exp \left[-4\ln 2 \left(\frac{t-2t_l}{t_l} \right)^2 \right] \quad (7)$$

where σ is an increment (real number); γ represents the thermal diffusivity of Au; α is equal to $1/\tau$, where τ is the relaxation time of the laser–Au interaction (1 ps); and t is the time, while t_l depicts the irradiation time of 1 fs and T_e is the electron temperature.

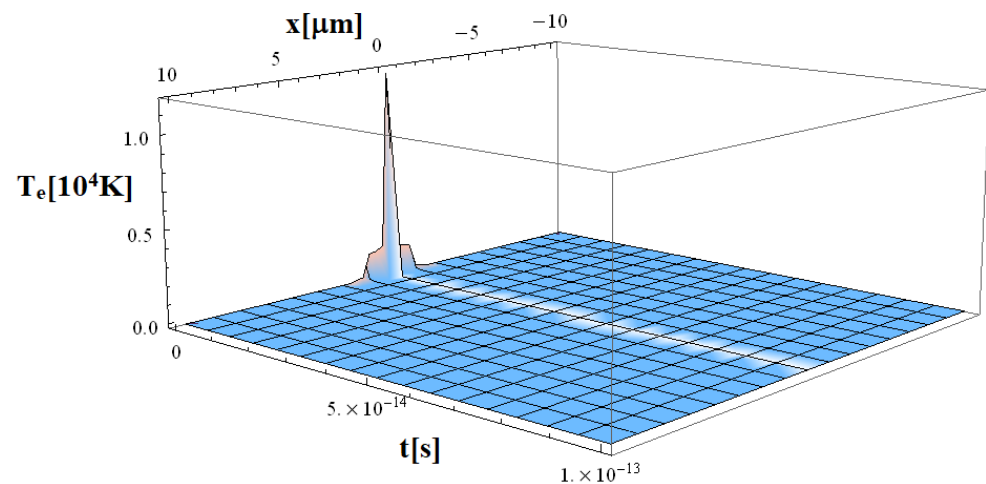


Figure 1. Electron temperature for an incident laser pulse with 1 fs duration with Gaussian spatial distribution.

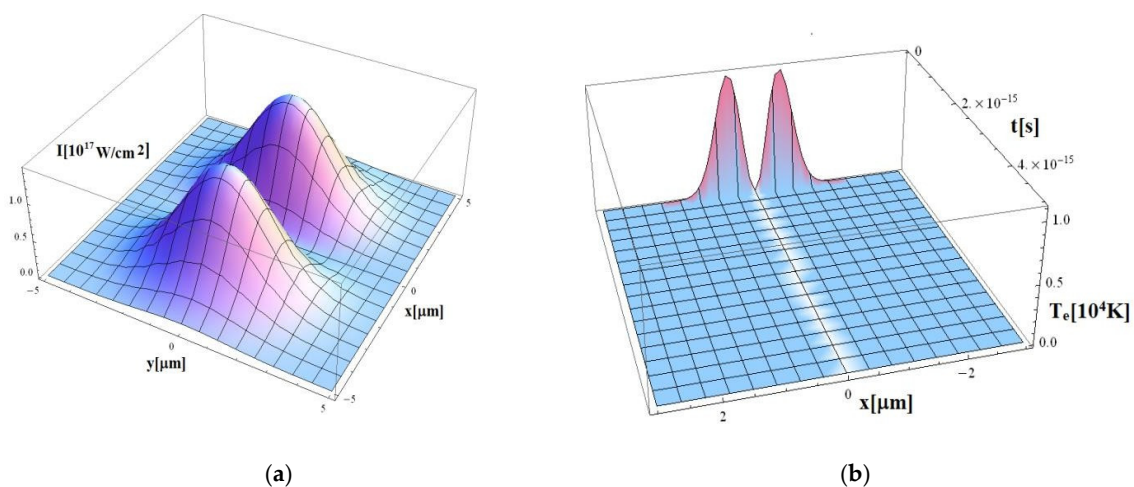


Figure 2. (a) Laser intensity, which acts in a transversal way (TEM_{01}), and (b) electron temperatures when incident laser pulse of 1 fs duration was considered to have a transversal TEM_{01} distribution.

The solution (Equation (6)) to the heat equation (Equation (5)) was tested in two analytical examples. An incident laser pulse with a 1 fs duration was considered to reach a laser power density of 10^{17} W/cm² and a Gaussian spatial distribution in the first case and a transversal (TEM₀₁) distribution in the second one. The results of the analytical simulations are represented in Figures 1–5, where T is measured in 10⁴ K.

A remarkable similarity is observed between the intensity and electron temperature distributions. This similitude provides convincing proof in favor of Equation (6), which can predict the thermal field/electron temperature distribution in a plausible, pertinent manner, with values close to the actual ones at the irradiation site.

One notices an excellent concordance between our results in Figures 1 and 2 and other experimental and numerical models [1]. Thus, in the particular case of Au, the temperature range of (5×10^3 – 10^4) K predicted by our simulations is in good agreement with the results obtained under irradiation with pulses of 5 TW/cm² intensity.

3. Mathematical Modeling of Lattice/Phonon Temperature Field

Next, we consider the laser heating of a semi-infinite metallic target for incident intensities of up to 10^{17} W/cm² and the application of the Fokker–Planck formalism, which is a stronger version of the one presented by Zhukovsky [23]. In order to analytically solve the Fokker–Planck equation, the Zhukovsky–Dattoli treatment was employed. This procedure was extended to calculate the lattice temperature, T_l , after irradiation with a 1 fs laser pulse.

In this case, the inferred heat equation takes the following form:

$$\frac{\partial T_l(x, t)}{\partial t} = \frac{\partial^2 T_l(x, t)}{\partial x^2} + \beta x T_l(x, t) \quad (8)$$

where β is a coefficient indicating the proportion of the non-diffusive phenomenon; the phenomenon is purely non-diffusive when $\beta = 1$ and purely diffusive when $\beta = 0$.

The initial conditions in this case are written as follows: $T_l(x, 0) = f(x)$, while $T_l(x, 0) = f(x) = \langle T_e \rangle$. This actually means that $\langle T_e \rangle$ constitutes the source term for the second (lattice) TTM heat equation ($\langle T_e \rangle$ stands for the mean value of the electron temperatures).

Accordingly, the corresponding solutions of Equations (1) and (2) in this case are as follows:

$$T_l(x, t) = e^{\varphi(x, t, \beta)} \frac{1}{2\sqrt{\pi t}} \int_{-\infty}^{+\infty} d\tilde{\xi} e^{-\frac{(x + \beta t^2 - \tilde{\xi})^2}{4t}} f(\tilde{\xi}) \quad (9)$$

$$\varphi(x, t, \beta) = \frac{1}{3}\beta^2 t^3 + \beta t x \quad (10)$$

Here, ξ is an increment (real number) and φ is a phase function defined by Equation (10).

4. Results and Discussion: Diffusion and Non-Diffusive Phonons

Figures 1 and 2a,b illustrate the evolution of the computed electron temperatures in the TTM for incident pulses with 1 fs durations. One should notice that the analyses in both [6] and the new model are based upon the application of a Fourier approach, according to which the thermal waves propagate with an infinite velocity. This allows for a more realistic description of electron temperatures for 1 fs than 100 fs in [6] because the heat propagation velocity is closer, in the first case, to the speed of light in a vacuum, if not to infinity. It is also why the thermal distribution of electrons bears, in this case, the “im-print” of the source term for the difference in [6].

One can further obtain the mode-resolved phonon temperatures using a 20 nm thick Au thin film by excluding/including phonon–phonon coupling. The lattice temperature (T_l) in the two cases is further used as a guiding value.

To assign the difference between the two cases more clearly, three representative phonon modes have been selected from the (three) phonon categories. They have MFPs

of 100, 5, and 1 nm, representing the non-diffusive, semi-diffusive, and diffusive phonon modes, respectively.

Simulation results of the lattice/phonon temperature (T_l), namely, Equations (9) and (10) for the three cases of interest (i.e., for different values of parameter β), are displayed in Figures 3–6. Here, z is the depth into the thin film and L is the total thickness of 20 nm. The application of the Fokker–Planck formalism in this case allows for clear discrimination between diffusive and non-diffusive phenomena.

A pure typical diffusive case is visible in Figure 3.

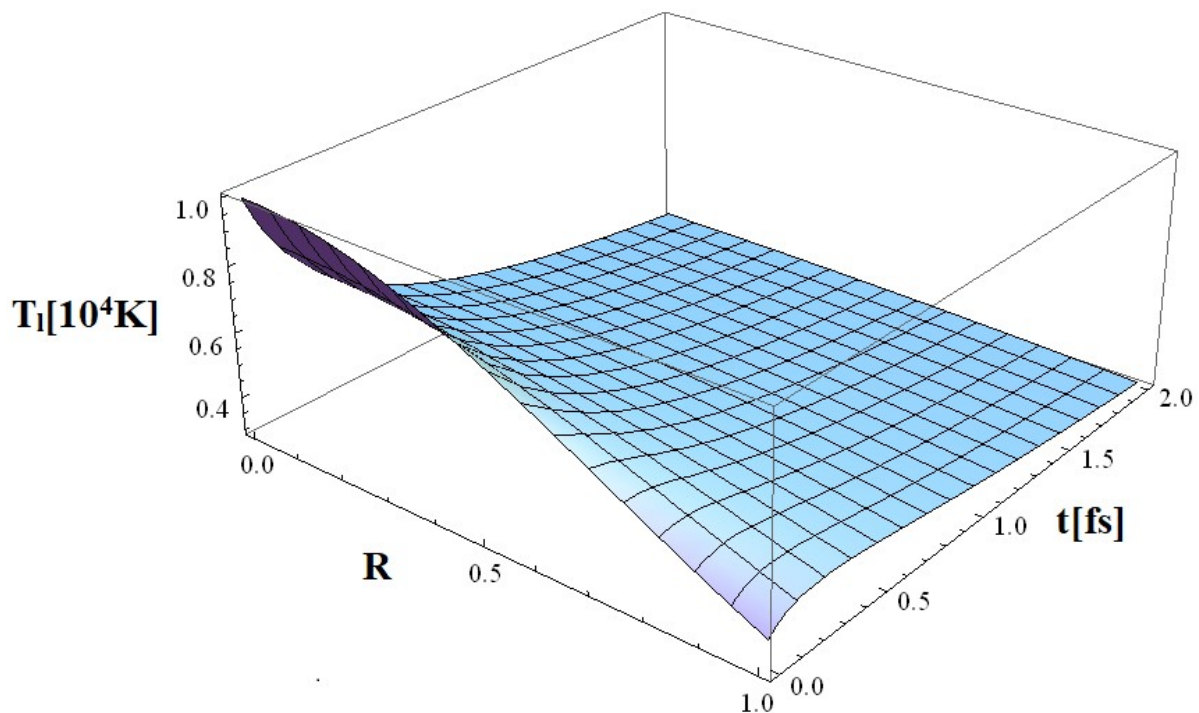


Figure 3. The lattice temperature distribution relating to $\beta = 0$, i.e., the case when the mean free pass, which coincides with the wavelengths of phonon collisions, is much larger than the target dimensions, a situation known as the diffusion case.

Figure 4 corresponds to the situation when the diffusion length is almost equal to the target dimensions, a situation described as a semi-diffusion case. This is precisely the case of the Au target in our study (of ~38 nm) [18]. It is notable that in this case β is equal to 0.4.

In Figure 5, the wavelength of a phonon is much larger than the target dimension but the thermal field becomes saturated for a constant value, a case that is described as non-diffusive. The β parameter in this case is 0.6.

Figure 6 presents the totally non-diffusive case, when the β parameter is 1. The reality is always between the extreme cases, when both diffusive and non-diffusive phenomena are simultaneously presented, like in Figures 4 and 5.

The information available in Figures 3–6 has been confirmed by many other simulations, so one may conclude that the β parameter plays a key role in determining the difference between the diffusive and non-diffusive mechanisms.

Both cases (with and without phonon–phonon coupling) share common features. First, they both predict large local non-equilibrium phonon temperatures, i.e., different phonon modes with different T_l values at the same location, in agreement with the molecular dynamics (MD) simulation results [24]. Second, the temperature of the non-diffusive phonon deviates the most in the two cases from the lattice temperature and exhibits an almost flat profile, i.e., a small temperature gradient. Third, the boundary temperature (on the hot side) of each phonon mode increases evenly when decreasing the MFP, meaning

that the more diffusive phonons exhibit a higher temperature on the hot side but a lower one on the cold side. Fourth, the lattice temperatures are comparable in the two cases.

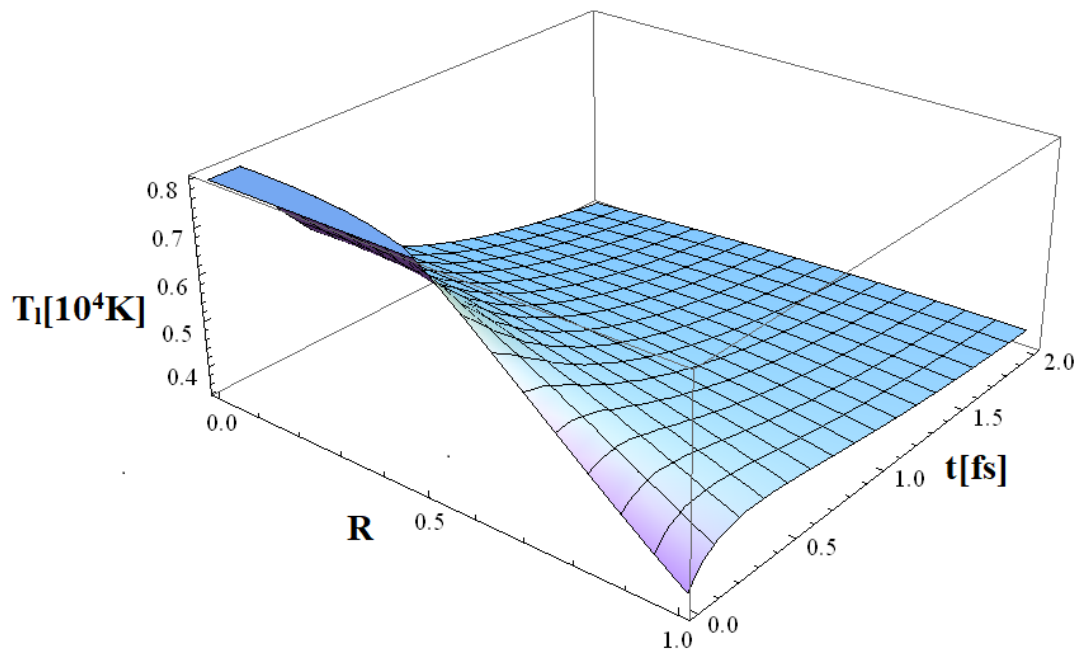


Figure 4. The lattice temperature distribution corresponds to $\beta = 0.4$, i.e., the situation when the diffusion length is almost equal to the target dimensions, a situation described as a semi-diffusion case.

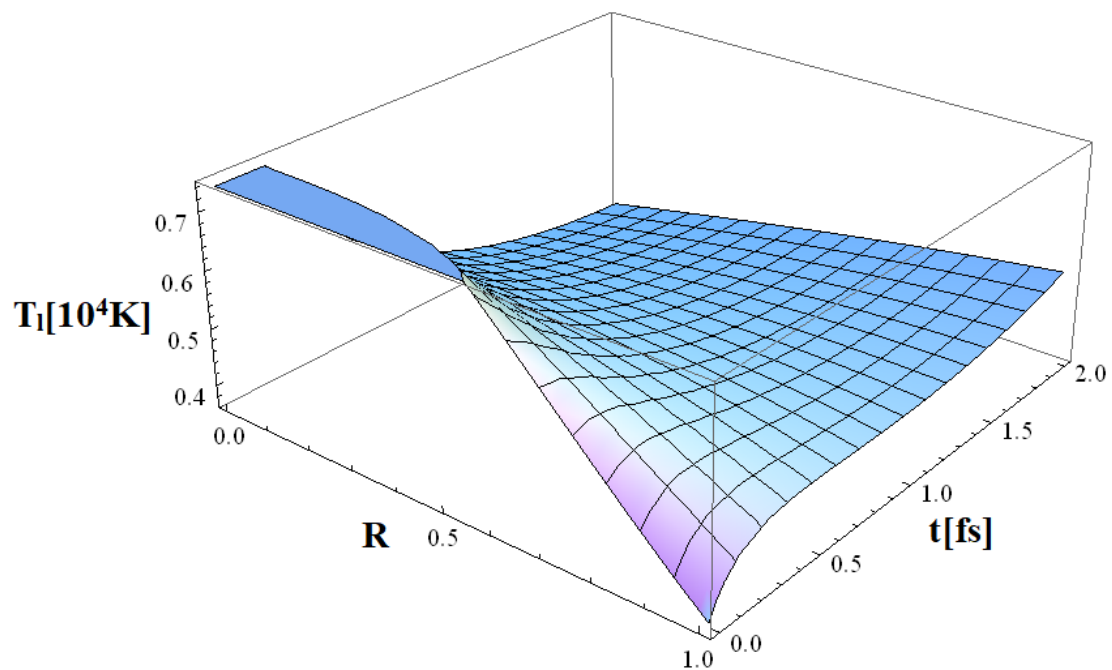


Figure 5. The lattice temperature distribution corresponding to $\beta = 0.6$, when the wavelength of a phonon is much larger than the target dimension but the thermal field saturates for a constant value, a case that is known as non-diffusive.

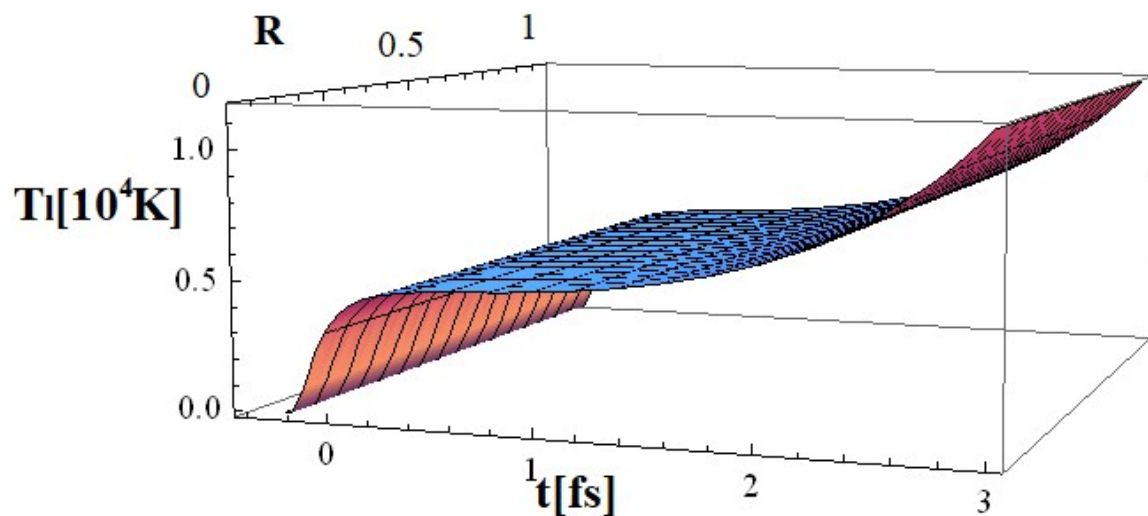


Figure 6. The lattice temperature distribution corresponding to $\beta = 1$, the totally non-diffusive case.

There are, however, major differences between the two cases. Thus, the phonon temperature gradient increases evenly when decreasing the MFP in the case of no phonon–phonon coupling. The order is $\nabla T_{\text{diffusive}} > \nabla T_{\text{semi-diffusive}} \sim \nabla T_l > \nabla T_{\text{non-diffusive}}$. This is due to the longer MFPs of non-diffusive phonons, which support fewer collisions or less energy loss after a certain distance [19]. Due to the truly short duration of irradiation, we do not have a phonon–phonon coupling factor [19]. Finally, we should mention that our model loses any physical significance for a β superior to unity.

The proposed model can be extended to other metal targets with similar thermal behavior: Al, Ag, Cu, Zn, and so on.

Indeed, according to Figure 12 in Ref [1], the thermal spectra in the TTM for Au, Cu, and Al have similar behaviors. This refers to either the electron or phonon temperature in the entire fs–ps range. A higher phonon temperature is, however, observed for Au, which might be due to its superior mass density with respect to other metals.

These analyses could be coupled to other thermal models that focus on monitoring the temperature and status (diffusive or non-diffusive) of phonons. Examples are models based on Boltzmann or Fourier equations, molecular beam dynamics, or memory versions of Fokker–Planck equations [19,25].

5. Conclusions

1. A generalized model was elaborated to describe the electron temperature field in the case of metal (Au) irradiation with 1 fs multi-mode laser pulses. A remarkable relationship was shown between the laser beam intensity distribution at the irradiation spot and the electron temperature field on and beneath the target surface.
2. An analytical Fokker–Planck model was developed in order to describe the lattice/phonon temperature under the same irradiation conditions using a parameter (β) that has values within the 0–1 range, corresponding to the transition from the diffusive phonon case to the non-diffusive phonon case. It should be noted that outside the range of 0–1 the model generates nonsensical situations.
3. The model is simple, versatile, and can be operated on a commercial PC. The simulation time using the MATHEMATICA 11.00 software package is generally less than 20 s, which is much shorter than the Monte Carlo simulation, which may take hours. Details of solving a heat equation via a semi-analytical approach are provided in Ref. [26].
4. It should be mentioned that the two-temperature model, which was initially designed to describe laser–metal interactions, was extended in recent years to be generalized to laser–solid interactions [27–31].

Author Contributions: Conceptualization: M.O. and I.N.M.; Data curation: M.O.; Formal analysis: M.O., I.N.M., A.M.I.T., B.A.S. and A.V.F.; Funding acquisition: I.N.M. and C.N.M.; Investigation: M.O., A.M.I.T., B.A.S., C.R., S.-A.A., N.M. and M.E.; Methodology: M.O., I.N.M., C.R., N.M. and M.E.; Project administration: I.N.M. and C.N.M.; Resources: I.N.M. and C.N.M.; Software: M.O., D.T. and C.R.; Supervision: M.O., I.N.M., A.M.I.T., B.A.S. and C.N.M.; Validation: M.O., I.N.M., A.M.I.T., B.A.S., A.V.F. and M.E.; Visualization: M.O., I.N.M., A.M.I.T., B.A.S. and N.M.; Writing—original draft: M.O., I.N.M., A.M.I.T., B.A.S., A.V.F. and S.-A.A.; Writing—review and editing: M.O., I.N.M., A.M.I.T., B.A.S., A.V.F., C.R. and M.E. All authors have read and agreed to the published version of the manuscript.

Funding: This work was supported under the contracts PN-III-P4-ID-PCE-2020- 2030 (PCE113/2021). This research was supported by the Romanian Ministry of Research, Innovation and Digitalization under Romanian National Nucleu Program LAPLAS VII (contract No. 30N/2023) and through Program I—Development of the National R&D System, Subprogram 1.2—Institutional Performance—Projects for Excellence Financing in RDI (contract No. 13PFE/2021); the Core Program, granted by the Romanian Ministry of Research, Innovation and Digitalization (MRID) through the contract OPTRONICA VII (No. 11N/2023); and MRID through Program I—Development of the National R&D System, Subprogram 1.2—Institutional Performance—Projects for Excellence Financing in RDI (contract No. 18PFE/2021).

Data Availability Statement: Not applicable.

Conflicts of Interest: The authors declare no conflict of interest.

References

- Li, X.; Guan, Y. Theoretical fundamentals of short pulse laser–metal interaction: A review. *Nanotechnol. Precis. Eng.* **2020**, *3*, 105–125. [\[CrossRef\]](#)
- Eugene, G. Gamaly and Saulius Juodkazis, Laser–Metal Interaction with a Pulse Shorter than the Ion Period: Ablation Threshold, Electron Emission and Ion Explosion. *Nanomaterials* **2023**, *13*, 1796. [\[CrossRef\]](#)
- DePond, P.J.; Fuller, J.C.; Khairallah, S.A.; Angus, J.R.; Guss, G.; Matthews, M.J.; Martin, A.A. Laser-metal interaction dynamics during additive manufacturing resolved by detection of thermally-induced electron emission. *Commun. Mater.* **2020**, *1*, 92. [\[CrossRef\]](#)
- Prokhorov, A.M.; Ursu, I.; Konov, V.I.; Mihailescu, I.N. *Laser Heating of Metals*, 1st ed.; Prokhorov, A.M., Ed.; Adam Hilger Ltd.—The Publishing House of the Institute of Physics: Bristol, UK, 1990.
- Norton, D.P. Pulsed Laser Deposition of Complex Materials: Progress Toward Applications. In *Pulsed Laser Deposition of Thin Films: Applications-Led Growth of Functional Materials*; Eason, R., Ed.; John Wiley & Sons: New York, NY, USA, 2007; pp. 1–31. [\[CrossRef\]](#)
- Nicarel, A.; Oane, M.; Mihailescu, I.N.; Ristoscu, C. Fourier two-temperature model to describe ultrafast laser pulses interaction with metals: A novel mathematical technique. *Phys. Lett. A* **2021**, *392*, 127155. [\[CrossRef\]](#)
- Anisimov, S.I.; Kapeliovich, B.L.; Perel'man, T.L. Electron emission from metal surfaces exposed to ultrashort laser pulses. *J. Esp. Teor. Phys.* **1974**, *66*, 776–781.
- Naqvi, K.R.; Waldenström, S. Brownian Motion Description of Heat Conduction by Phonons. *Phys. Rev. Lett.* **2005**, *95*, 065901. [\[CrossRef\]](#) [\[PubMed\]](#)
- Kautek, W.; Armbruster, O. Non-Thermal Material Response to Laser Energy Deposition. In *Lasers in Materials Science*; Castillejo, M., Ossi, P.M., Zhigilei, L., Eds.; Springer Series in Materials Science: Cham, Switzerland, 2014; Volume 191, pp. 43–66. [\[CrossRef\]](#)
- Fann, W.S.; Storz, R.; Tom, H.W.K.; Bokor, J. Direct measurement of nonequilibrium electron-energy distributions in subpicosecond laser-heated gold films. *Phys. Rev. Lett.* **1992**, *68*, 2834–2837. [\[CrossRef\]](#)
- Mueller, B.Y.; Rethfeld, B. Relaxation dynamics in laser-excited metals under nonequilibrium conditions. *Phys. Rev. B* **2013**, *87*, 035139. [\[CrossRef\]](#)
- Ndione, P.D.; Gericke, D.O.; Rethfeld, B. Optical Properties of Gold After Intense Short-Pulse Excitations. *Front. Phys.* **2022**, *10*, 856817. [\[CrossRef\]](#)
- Lizunov, S.A.; Bulgakov, A.V.; Campbell, E.E.B.; Bulgakova, N.M. Melting of gold by ultrashort laser pulses: Advanced two-temperature modeling and comparison with surface damage experiments. *Appl. Phys. A* **2022**, *128*, 602. [\[CrossRef\]](#)
- Demaske, B.J.; Zhakhovsky, V.V.; Inogamov, N.A.; Oleynik, I.I. Ablation and spallation of gold films irradiated by ultrashort laser pulses. *Phys. Rev. B* **2010**, *82*, 064113. [\[CrossRef\]](#)
- Arefev, M.I.; Shugaev, M.V.; Zhigilei, L.V. Kinetics of laser-induced melting of thin gold film: How slow can it get? *Sci. Adv.* **2022**, *8*, eabo2621. [\[CrossRef\]](#) [\[PubMed\]](#)
- Gurevich, E.L.; Levy, Y.; Gurevich, S.V.; Bulgakova, N.M. Role of the temperature dynamics in formation of nanopatterns upon single femtosecond laser pulses on gold. *Phys. Rev. B* **2017**, *95*, 054305. [\[CrossRef\]](#)

17. Petrov, G.M.; Davidson, A.; Gordon, D.; Peñano, J. Modeling of short-pulse laser-metal interactions in the warm dense matter regime using the two-temperature model. *Phys. Rev. E* **2021**, *103*, 033204. [[CrossRef](#)] [[PubMed](#)]
18. Joshi, A.A.; Majumdar, A. Transient ballistic and diffusive phonon heat transport in thin films. *J. Appl. Phys.* **1993**, *74*, 31–39. [[CrossRef](#)]
19. Xu, J.; Hu, Y.; Ruan, X.; Wang, X.; Feng, T.; Bao, H. Nonequilibrium phonon transport induced by finite sizes: Effect of phonon-phonon coupling. *Phys. Rev. B* **2021**, *104*, 104310. [[CrossRef](#)]
20. Torres, P.; Royo, M.; López-Suárez, M.; Shiomi, J.; Rurali, R. Quasiballistic phonon transport from first principles. *Phys. Rev. B* **2020**, *102*, 144305. [[CrossRef](#)]
21. Diao, C.; Yang, Z.; Dong, Y.; Duan, Y. Ballistic-diffusive phonon transport and thermal rectification across single-molecule junctions. *Int. J. Heat Mass Transf.* **2020**, *157*, 119851. [[CrossRef](#)]
22. Mihăilescu, C.N.; Oane, M.; Mihăilescu, N.; Ristoscu, C.; Mahmood, M.A.; Mihăilescu, I.N. A New Approach to Solve Non-Fourier Heat Equation via Empirical Methods Combined with the Integral Transform Technique in Finite Domains. In *Matrix Theory—Classics and Advances*; IntechOpen: Rijeka, Croatia, 2022; pp. 1–11. [[CrossRef](#)]
23. Zhukovsky, K.; Dattoli, G. Evolution of non-spreading Airy wavepackets in time dependent linear potentials. *Appl. Math. Comput.* **2011**, *217*, 7966–7974. [[CrossRef](#)]
24. Shugaev, M.V.; Wu, C.; Armbruster, O.; Naghilou, A.; Brouwer, N.; Ivanov, D.S.; Derrien, T.J.-Y.; Bulgakova, N.M.; Kautek, W.; Rethfeld, B.; et al. Fundamentals of ultrafast laser–material interaction. *MRS Bull.* **2016**, *41*, 960–968. [[CrossRef](#)]
25. Maassen, J.; Lundstrom, M. Steady-state heat transport: Ballistic-to-diffusive with Fourier’s law. *J. Appl. Phys.* **2015**, *117*, 035104. [[CrossRef](#)]
26. Oane, M.; Mahmood, M.A.; Popescu, A.C. A State-of-the-Art Review on Integral Transform Technique in Laser–Material Interaction: Fourier and Non-Fourier Heat Equations. *Materials* **2021**, *14*, 4733. [[CrossRef](#)]
27. Abbas, I.; Saeed, T.; Alhothuali, M. Hyperbolic Two-Temperature Photo-Thermal Interaction in a Semiconductor Medium with a Cylindrical Cavity. *Silicon* **2021**, *13*, 1871–1878. [[CrossRef](#)]
28. Jarrin, T.; Jay, A.; Hémerlyck, A.; Richard, N. Parametric study of the Two-Temperature Model for Molecular Dynamics simulations of collisions cascades in Si and Ge. *Nucl. Instrum. Methods Phys. Res. Sect. B Beam Interact. Mater. Atoms* **2020**, *485*, 1–9. [[CrossRef](#)]
29. Alzahrani, F.; Abbas, I. The Effect of a Hyperbolic Two-Temperature Model with and without Energy Dissipation in a Semiconductor Material. *Mathematics* **2020**, *8*, 1711. [[CrossRef](#)]
30. Gonzalez-Narvaez, R.E.; de Haro, M.L.; Vázquez, F. Internal Structure and Heat Conduction in Rigid Solids: A Two-Temperature Approach. *J. Non-Equilib. Thermodyn.* **2022**, *47*, 13–30. [[CrossRef](#)]
31. Zenkour, A.M.; Abouelregal, A.E. Two-temperature theory for a heated semi-infinite solid by a pulsed laser radiation. *Arch. Thermodyn.* **2020**, *41*, 85–101. [[CrossRef](#)]

Disclaimer/Publisher’s Note: The statements, opinions and data contained in all publications are solely those of the individual author(s) and contributor(s) and not of MDPI and/or the editor(s). MDPI and/or the editor(s) disclaim responsibility for any injury to people or property resulting from any ideas, methods, instructions or products referred to in the content.